

# Multilevel Graph Partitioning for Three-Dimensional Discrete Fracture Network Flow Simulations

Hayato Ushijima-Mwesigwa<sup>1</sup>, Jeffrey D. Hyman<sup>\*2</sup>, Aric Hagberg<sup>3</sup>, Ilya Safro<sup>1</sup>, Satish Karra<sup>2</sup>, Carl W. Gable<sup>2</sup>, and Gowri Srinivasan<sup>4</sup>

<sup>1</sup>*School of Computing, Clemson University, Clemson, South Carolina, USA*

<sup>2</sup>*Computational Earth Science (EES-16), Earth and Environmental Sciences Division, Los Alamos National Laboratory, Los Alamos New Mexico, USA*

<sup>3</sup>*Computer, Computational, and Statistical Sciences Division, Los Alamos National Laboratory, Los Alamos New Mexico, USA*

<sup>4</sup>*Verification and Analysis (XCP-8), X Computational Physics, Los Alamos National Laboratory, Los Alamos New Mexico, USA*

## Abstract

We present a topology-based method for mesh-partitioning in three-dimensional discrete fracture network (DFN) simulations that takes advantage of the intrinsic multi-level nature of a DFN. DFN models are used to simulate flow and transport through low-permeability fracture media in the subsurface by explicitly representing fractures as discrete entities. The governing equations for flow and transport are numerically integrated on computational meshes generated on the interconnected fracture networks. Modern high-fidelity DFN simulations require high-performance computing on multiple processors where performance and scalability depends partially on obtaining a high-quality partition of the mesh to balance work work-loads and minimize communication across all processors.

The discrete structure of a DFN naturally lends itself to various graph representations, which can be thought of as coarse-scale representations of the computational mesh. Using this concept, we develop a variant of the multilevel graph partitioning algorithm to partition the mesh of a DFN. We compare the performance of this DFN-based mesh-partitioning with standard multi-level graph partitioning using graph-based metrics (cut, imbalance, partitioning time), computational-based metrics (FLOPS, iterations, solver time), and total run time. The DFN-based partition and the mesh-based partition are comparable in terms of the graph-based metrics, but the time required to obtain the partition is several orders of magnitude faster using the DFN-based partition. The computation-based metrics show comparable performance between both methods so, in combination, the DFN-based partition is several orders of magnitude faster than the mesh-based partition.

## 1 Introduction

Discrete Fracture Network (DFN) models are a computational tool for modeling flow and transport through low-permeability subsurface fractured rock. DFN models differ from conventional continuum models by explicitly representing fractures and the networks they form. This allows DFNs to represent a wider range of transport phenomena and makes them a preferred choice when linking network attributes to flow properties [24, 35]. DFNs are utilized for characterizing fluid flow and solute transport through low permeability

---

\*corresponding author: jhyman@lanl.gov

fractured media which is critical for a variety of subsurface applications including the environmental restoration of contaminated fractured media [57, 59, 75], aquifer storage and management [44], hydrocarbon extraction [36, 41, 53], longterm storage of spent civilian nuclear fuel [20, 24, 40], and CO<sub>2</sub> sequestration [39].

The choice to explicitly represent fractures results in a significantly higher computational cost than stochastic continuum [59] or dual porosity/permeability [47] models where upscaled effective properties are used to account for fracture properties. Once a network is constructed, the individual fractures are meshed for computation and the governing equations for flow and transport are numerically integrated on the computational mesh. The number of mesh cells required for a DFN depends on the number of fractures, the density of the network, and the range of length scales being resolved. Even modest sized DFNs containing  $O(10^2)$  fractures can have a mesh that contains several million nodes. Because of limited computational resources, the first DFN models either represented networks as a set of connected pipes [10, 16] or were two-dimensional representations [14]. Despite the large scale of DFN computations, high performance computing (HPC) enables flow and transport simulations in large three-dimensional DFNs [4, 5, 17, 38, 55, 61, 62].

These high-fidelity DFN simulations require HPC on multiple processors and the performance and scalability of these simulations necessitate a high-quality partitioning such that the computations are well-balanced across all processes with minimal communication between processors. Common partitioning methods [9] are based on either a global method, e.g., spectral partitioning and max-flow, or iterative local improvement heuristic algorithms, e.g., Kernighan-Lin [43] or Fiduccia-Matthesyses [19]. However, multilevel graph partitioning, which introduces a framework to make global decisions in conjunction with local improvements, is one of the most successful heuristics in practice for partitioning large graphs [12, 42, 66, 69, 70, 77].

The basic idea behind multilevel graph partitioning is that a graph is successively coarsened, creating a hierarchy of smaller graphs until an initial (coarsest) partition can be computed efficiently. The initial partition is projected back to the next finer level, where local improvements are made. Once at a local optima, the improved partition is projected to the next finer level where further local improvement are made. The process continues until a partition is projected and refined back to the original graph. Multilevel graph partitioning methods are popular because they exhibit excellent trade-off between fast computational time and high-quality solutions compared to other techniques. However, some applications (for example those involving dynamic graphs) require graphs to be repartitioned, and thus require much faster techniques. Thus, depending on the application, even multilevel graph partitioning can take a significant amount of time.

To increase the speed of high-resolution DFN simulations, we propose an approach to graph partitioning the DFN mesh that combines the topological structure of the DFN with multilevel graph partitioning. The discrete structure of a DFN naturally lends itself to various graph representations, for example, vertices in graph can correspond to fractures in the DFN and edges in the graph to fracture intersections. These graph-representations of a DFN can also be thought of as coarse-scale representations of the computational mesh, which is the conceptual model that we use here to develop a variant of the multilevel graph partitioning algorithm for mesh partitioning. By using this partitioning on the DFN, we seek to accelerate the HPC computations. The proposed methodology assigns the first coarse level in the multilevel graph partitioning to be a weighted graph based on the topology of the DFN that accounts for the number of mesh nodes on each fracture.

We compare the relative cost of the proposed method with partitioning the full mesh and find that the total run time is reduced by several orders of magnitude using the proposed method. Partitioning the graph-representation of the DFN and projecting the solution onto the mesh is computationally cheaper than partitioning the DFN mesh itself since there are orders of magnitude fewer nodes and edges to consider in a graph based on the DFN topology. The method is also sensitive to the mesh resolution on each fracture, i.e., it accounts for the number of mesh nodes on each fracture. The performance of the method compared to partitioning the mesh is measured in terms of graph-based metrics (cut, imbalance, partitioning time), computational-based metrics (FLOPS, iterations, solver time), and total run time. In terms of graph-based metrics, the results obtained using the DFN-based partition are comparable to those obtained using the mesh-

based partition, yet the DFN-based partition is several orders of magnitude faster. The results presented here indicate that using the proposed method overall reduces the required time for a single DFN realization simulation and thus allows one to perform more realizations for uncertainty quantification, for a fixed computational budget.

## 2 Discrete Fracture Networks

In low-permeability fractured media like shale and crystalline rock, fluid flow and the associated transport of solutes is mainly confined to the fractures embedded in the medium [57]. In these physical systems, the structure of the fluid velocity field therein is primarily controlled by the geometry of individual fractures, e.g., size and aperture, and the structure of the network as opposed to matrix properties, e.g., matrix porosity or pore-size distributions [13, 15, 35, 32]. There are a number of methods used to model flow and the associated transport of chemical species including stochastic continuum [58, 59, 73], dual-porosity / dual-permeability [23, 78, 47], and discrete fracture network model (DFN) [10, 48, 49, 50, 60].

In the DFN methodology, individual fractures are represented as planar  $N - 1$  dimensional objects embedded within an  $N$  dimensional space, lines in two dimensions and planes in three dimensions. The size of the domains of interest and the cost of sufficiently sampling relevant quantities in the subsurface, both hydraulic and structural, result in limited availability of data [6, 57, 78] and requires that DFN models are constructed stochastically. Each fracture within the network is assigned a shape, location, and orientation within the domain by sampling distributions whose parameters are determined by a site characterization [40]. The fractures form a network embedded within the porous medium that are meshed for computation and the governing equations for flow and transport are numerically integrated to simulate physical phenomenon of interest.

The stochastic generation of a DFN is a major obstacle in the creation of a high-quality computational mesh representation of each network. In practice, the planes representing each fracture are randomly included into the domain and can create arbitrarily small features, i.e., length scales, that render the automated meshing of the fracture plans infeasible. Figure 1 shows a DFN composed of 424 fractures in a 15 meter cube, which are represented as circular polygons, to demonstrate the range of length scales that exists in a DFN. Colors on the fractures correspond to the distance on the fracture to the nearest line of intersection and highlight the range of length scales that exists on a fracture plane and throughout the network. Mesh edges must be smaller than the smallest length scale in the network if the physics are to be properly resolved. This requirement is computationally infeasible for arbitrarily small length scales within large domains. There have been a number of methodologies to address this issue by modifying the mesh to remove small features [56, 55] or coupling flow between non-conforming meshes using discretization schemes [4, 17, 61, 62].

### 2.1 Meshing Strategy FRAM

The Feature Rejection Algorithm for Meshing (FRAM) introduced by Hyman et al. [33] is one method designed to address the aforementioned mesh generation issues. The cornerstone of FRAM is a user-defined minimum length scale ( $h$ ) that determines what geometric features are represented in the network. FRAM constrains the generation of the network so that the smallest feature is greater than  $h$  through the entire network. This constraint provides a firm lower bound on the required resolution of the mesh and ensures that pathological cases, e.g., arbitrarily small intersections and distances between intersections, that degrade mesh quality do not exist. Then all the features in the network can be resolved by generating triangular cell edges with a minimum length slightly less than  $\approx h/2$ . Once these constraints are met, a conforming Delaunay triangulation algorithm [54] is implemented to mesh each fracture in a manner such that all lines of intersection form a set of connected edges in the Delaunay triangulation. The dual of the Delaunay triangulation

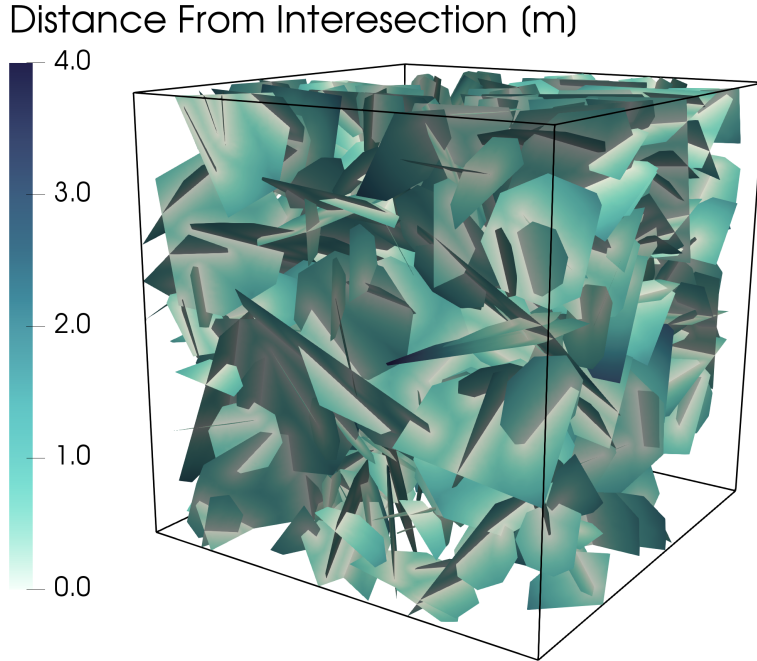


Figure 1: A Discrete Fracture Network (DFN) composed of 424 fractures in a 15 meter cube. Colors correspond to the distance on the fracture plane to the nearest fracture intersection. The regions colored white are close to fracture intersections and darker colors indicate larger distances. The variability in colors on a single plane highlights the range of length scales that exist on a single fracture and throughout the network. To properly simulate relevant physical phenomenon the mesh representation of the network must be fine enough to resolve all of these length scales.

is a Voronoi tessellation, which in a certain sense is optimal for two-point flux finite volume solvers [18], that are commonly used in subsurface flow and transport simulators such as FEHM [79], TOUGH2 [63], and PFLOTRAN [46].

One key aspect of FRAM is the provided detailed control of the mesh resolution on each fracture because pathological cases that degrade mesh quality do not exist. Depending upon the physical process to be simulated, the mesh can either have variable or uniform resolution. Points of singularity in the pressure solution occur at the ends of intersection lines and high gradients in the pressure solution and flow fields occur close to the intersections. To properly resolve these gradients the mesh needs to be finer in these regions. If fracture properties are homogeneous within a fracture, i.e., uniform fracture apertures, or only a pressure solution is required, or transport will be simulated using particle tracking then the mesh can be coarsened away from the intersections without significant loss of accuracy. However, if non-uniform apertures are considered, as in [15, 50], then the mesh needs to be sufficiently fine that length scales in the aperture field, e.g., correlation lengths, are resolved. Furthermore, if transport is simulated using an Eulerian approach, i.e., a numerical discretization of the advective-dispersion equation, where numerical diffusion/dispersion is controlled by the mesh resolution then a uniform mesh is more appropriate because numerical errors will be uniform across the domain.

Due to these considerations, we propose an extension of the FRAM to allow for variable mesh resolution

based on distance from the lines of intersection in a fracture. From a topological point of view, every DFN can be represented as a tuple consisting of a set of fractures and a set of intersections. Formally, let  $\mathcal{F} = \{f_i\}$  for  $i = 1, \dots, N$  denote a fracture network composed of  $N$  fractures ( $f_i$ ). Every  $f_i \in \mathcal{F}$  is assigned a shape, location, and orientation within the domain by sampling distributions whose parameters are determined by a site characterization. Every  $f_i \in \mathbb{R}^2$  but the network  $\mathcal{F} \in \mathbb{R}^3$ . Let  $I = \{(f_i, f_j)\}$  be a set of pairs associated with intersections between fractures; if  $f_i \cap f_j \neq \emptyset$  then  $(f_i, f_j) \in I$ . The number of intersections  $M = |I|$  depends on the particular shape, orientation, and geometry of the set of fractures in the network. We denote the line of intersection between  $f_i$  and  $f_j$  as  $\ell(f_i, f_j)$ . Using these sets, the topology of a DFN can be defined as the tuple  $(\mathcal{F}, I)$ .

Next, we compute the minimum distance from every point on a fracture  $\mathbf{x} \in f_i$  to the lines of intersection on that fracture,

$$d(\mathbf{x}) = \min_{\mathbf{y} \in \ell(f_i, f_j)} \|\mathbf{x} - \mathbf{y}\| \quad \forall j \text{ s.t. } (f_i, f_j) \in I. \quad (1)$$

The maximum edge length in the mesh at a given distance from an intersection, denoted  $\|e(\mathbf{x})\|_{\max}$ , is determined by a two parameter piecewise linear function

$$\|e(\mathbf{x})\|_{\max} = \begin{cases} ad(\mathbf{x}) + h/2 & d(\mathbf{x}) \leq rh, \\ (ar + 1/2)h & d(\mathbf{x}) > rh. \end{cases} \quad (2)$$

If an edge in the mesh is greater than  $\|e(\mathbf{x})\|_{\max}$ , then a new point is added to the mesh at the midpoint of that edge to split it in two. In practice, the edge spitting is done using Rivara refinement [64, 65].

A few remarks about the method: (i) the mesh is refined to  $\approx h/2$  along the lines of intersection, (ii) the slope parameter  $a$  controls the rate that the mesh is coarsened away from the intersection and ensures gradual refinement, (iii) the distance parameter  $r$  determines furthest distance from the intersections that the mesh resolution is variable, (iv) to make the mesh uniform, one can either set  $a = 0$  or  $r = 0$ .

Once the DFN is meshed, we can define the following functions

$$M_f : \mathcal{F} \rightarrow \mathbb{Z}^+, \quad (3)$$

returns the number of mesh nodes on a fracture  $f_i \in \mathcal{F}$  and

$$M_I : I \rightarrow \mathbb{Z}^+, \quad (4)$$

returns the number of mesh nodes on the line of intersection  $\ell(f_i, f_j) \in I$ . These functions allow us to consider the effects of different meshing strategies, uniform sized triangles compared to variable resolution, which we will use later in this study.

Figure 2 (a) provides a close up view of uniform mesh resolution on the network shown in Fig. 1 and Fig. 2 (b) shows a close view of variable mesh resolution in the same region. In Fig. 2 (b) the mesh is coarsened away from fracture intersections to reduce the overall size of the mesh using the method described above. The mesh shown in Fig. 2 (a) is composed of 870,685 nodes and 1,712,924 triangles while the mesh in (b) is made up of 360,912 nodes and 725,787 triangles.

### 3 Graph Partitioning

In HPC computations one wants to minimize the communication between processors and insure that the work performed on each processor is balanced. This problem of minimizing communication and load balancing is identical to the problem of partitioning the graph corresponding to the sparsity pattern of matrix  $A$  [45], which, in our problem, is equivalent to partitioning the mesh of the DFN. Thus, for a computer with  $k$  processors, we seek a partition of the graph based on the DFN mesh into  $k$  parts of equal size where the edges between those parts is minimized.

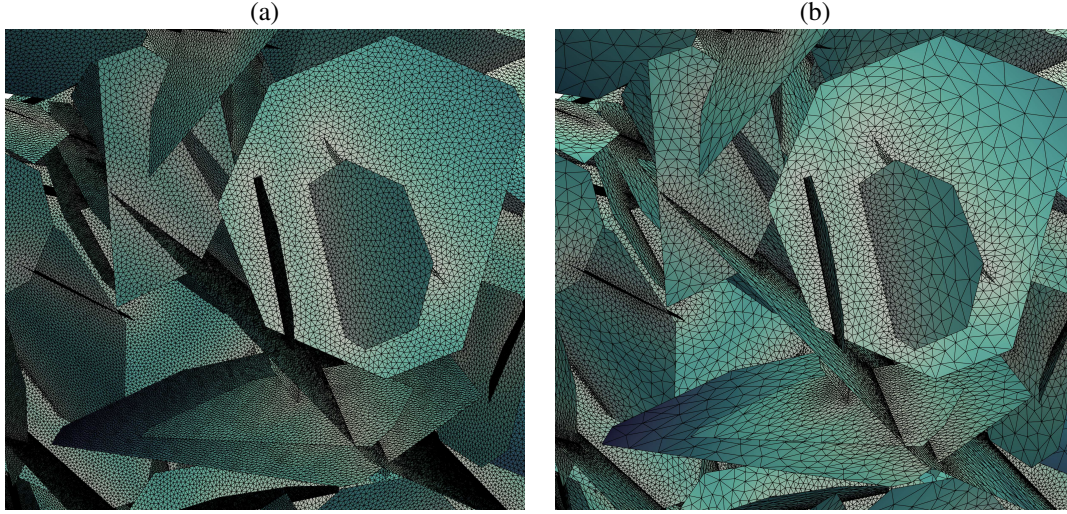


Figure 2: (a) Close view of uniform mesh resolution for the DFN shown in Fig. 1. (b) Close view of variable mesh resolution. In (b) the mesh is coarsened away from fracture intersections to reduce the overall size of the mesh. The mesh shown in (a) is composed of 870,685 nodes and 1,712,924 triangles while the mesh in (b) is made up of 360,912 nodes and 725,787 triangles.

### 3.1 $k$ -way Graph Partitioning

Formally, given a graph  $G = (V, E)$  composed of vertices  $u \in V$  and edges  $e_{i,j} = e(u_i, u_j) \in E$ , with non-negative vertex weights  $w_i : V \rightarrow \mathbb{R}^+$  and edge weights,  $w_{i,j} : E \rightarrow \mathbb{R}^+$  let  $P = (P_1, \dots, P_k)$ , be a partition of the vertex set  $V$  into  $k$  parts such that,

$$\cup_i P_i = V, \quad (5)$$

and

$$P_i \cap P_j = \emptyset \quad \text{for } i \neq j. \quad (6)$$

For a given partition we can measure the volume of each piece of the partition

$$|P_j| := \sum_{u_i \in P_j} w_i. \quad (7)$$

The volume of each piece of the partition is used to provide a measure of imbalance. For an imbalance parameter  $\varepsilon > 0$ , we can determine if  $P$  satisfies the balance constraint

$$\max_i |P_i| \leq (1 + \varepsilon) \left\lceil \frac{|W|}{k} \right\rceil, \quad (8)$$

where  $|W| = \sum_{v_i \in V} w_i$ . Moreover, we can also measure the cut of a partition

$$C(P) = \sum w_{i,j} \text{ s.t. } e_{ij} \in E, u_i \in P_k, u_j \in P_l \text{ and } k \neq l. \quad (9)$$

The  $k$ -way graph-partitioning problem (GP) is to find a  $k$ -partition,  $P$ , that satisfies the balance constraint (8) and minimizes the cut (9). In general, these two desires conflict with one another. Indeed, this graph partition problem is an NP-hard problem [22, 31].

### 3.2 Multilevel Graph Partitioning

Multilevel graph partitioning is one of the most successful heuristics for partitioning large graphs [8, 11, 21, 25, 27, 42, 51]. The idea behind multilevel graph partitioning originates from the multiscale optimization and multigrid strategies [7]. A graph is gradually coarsened to one where a  $k$ -way partition can be computed efficiently and effectively and then this partition is projected back onto the original graph. To be more specific, let us consider a weighted graph  $G_0 = (V_0, E_0)$  that has weights on both vertices and edges. Algorithm 1 summarizes the multilevel framework for graph partitioning.

**Input:** :  $G_0 = (V_0, E_0)$  with vertex weights  $w_i$  and edge weights  $w_{i,j}$ .

**Output:** :  $P(G)$

1. Coarsening phase : The graph  $G_0$  is transformed into a sequence of smaller graphs  $G_1, G_2, \dots, G_m$  such that  $|V_0| > |V_1| > |V_2| > \dots |V_m|$ .
2. Initial (coarsest graph) partitioning phase: a high-quality algorithm is employed to obtain a  $k$ -way partition  $P_m$  of the graph  $G_m = (V_m, E_m)$ .
3. Uncoarsening phase: The partition  $P_m$  of  $G_m$  is projected back to  $G_0$  via the intermediate partitions  $P_{m-1}, P_{m-2}, \dots, P_1, P_0$  which are refined at each level  $l \in [0, \dots, m-1]$ .

**Algorithm 1:** Multilevel Graph Partitioning

The approach consists of three main phases: (i) coarsening, (ii) initial partitioning and (iii) uncoarsening. In the *coarsening phase* the original graph ( $G_0$ ) is gradually approximated by creating a hierarchy of coarsened graphs,  $G_1, G_2, \dots, G_m$ , where there is a decreasing number of vertices in each graph  $|V_0| > |V_1| > |V_2| > \dots |V_m|$ . This can be achieved by collapsing edges and creating coarse level vertices, which are the nodes in the next level of the hierarchy that represent sets of vertices in next-coarser levels. The coarsening phase is stopped when the graph is small enough to be partitioned using an expensive but accurate algorithm. This phase is referred to as the *initial partitioning phase*. After the initial partitioning is performed, the *uncoarsening phase* begins, which is made up of two parts. In the first part of this stage, the partition at the coarser level  $P_i$  is projected onto the graph one level finer in the hierarchy  $G_{i-1}$ ,  $P_i \rightarrow P_{i-1}$ . Next, this projected partition is refined using a variant of the aforementioned improvement algorithms to create a better partition at this level in the hierarchy. This is done until  $P_0$  is obtained. There are other (sometimes more sophisticated) multilevel frameworks for partitioning [52, 69] and other cut-based problems on graphs such as the minimum linear arrangement [67], wavefront [29], bandwidth [68], and vertex separators [26].

## 4 DFN-based Graph Partitioning

In this section we describe one of the most common graph-representations of a DFN and develop methods to use that graph-representation in the partitioning of the mesh.

We adopt a graph representation of a DFN defined as a tuple  $(\mathcal{F}, I)$ , cf. Section 2.1, where vertices in the graph correspond to fractures in a  $\mathcal{F}$  and edges correspond to elements in the set of intersections  $I$ . Hyman et al. [37] recently showed that this particular graph-representation of a DFN is a projection of a more general bi-partite graph. A simple undirected graph  $F = (V_F, E_F)$  is constructed in the following way. For every  $f_i \in \mathcal{F}$ , there is a unique vertex  $u_i \in V_F$ ,

$$\phi : f_i \rightarrow u_i. \quad (10)$$

The vertex weight  $w_i$  for vertex  $u_i \in V_F$  is the number of mesh nodes on the fracture  $f_i$ , obtained using  $M_f$  (3),

$$w_i = M_f(f_i), \quad (11)$$

Edges are defined in the following way. If two fractures,  $f_i$  and  $f_j$  intersect,  $(f_i, f_j) \in I$ , then there is an edge in  $E$  connecting the corresponding vertices,

$$\phi : (f_i, f_j) \in I \rightarrow e_{ij} = (u_i, u_j), \quad (12)$$

where  $(u, v) \in E_F$  denotes an edge between vertices  $u$  and  $v$ . The edge weight  $w_{i,j}$  for vertex  $e(u_i, u_j) \in E_F$  is the number of mesh nodes on the edge  $(f_i, f_j) \in I$ , obtained using  $M_I$  (4),

$$w_{i,j} = M_I[(f_i, f_j)], \quad (13)$$

This particular mapping has been used by a variety of researchers [1, 2, 28, 30, 34, 35, 72, 74, 76].

Figure 3 shows a DFN composed of four fractures to demonstrate the connection between the graph-representation and the mesh. Figure 3(a) shows the DFN where each fracture has a unique color. Figure 3(b) shows the DFN with the mesh overlaid on the DFN, where the mesh colors correspond to the fracture on which they reside. Figure 3(c) shows the adopted graph-representation of the DFN where vertex colors coincide with the fracture colors and vertex size corresponds to the vertex weight. Figure 3(d) is a plot of the adjacency matrix of graph equivalent of the mesh where colors in the matrix correspond to the fractures on which the nodes reside. We perform a multi-index sort of the mesh nodes – first by fracture number, then x coordinate, y coordinate, and finally z coordinate. This sort reduces the bandwidth of the main diagonal of the adjacency matrix. The block structure of the mesh is a direct result of the fracture network topology, which is captured in the graph plot in Fig. 3(c). The mesh nodes on each fracture make up the main diagonal of the adjacency matrix in the plot shown in Fig. 3(d). The off diagonal nodes (black) correspond to mesh nodes along the fracture intersections. Each of these blocks corresponds to the a single vertex in graph shown in Fig. 3(c) and the number of non-zero entries in each block corresponds to the weight of the vertex. Mesh connections are mostly on a single fracture and there are fewer connections across fracture intersections, as indicated by the few off-diagonal terms in the adjacency matrix.

#### 4.1 Multilevel DFN-based Graph Partitioning

We now propose a variant of the multilevel graph partitioning algorithm that takes advantage of the topology of a DFN. The basic idea behind the method is to perform the partitioning on a graph based on the topology of the DFN and then projecting the resulting partition onto the DFN mesh.

Hyman et al. [37] showed that the graph representation  $F$  defined by equations (10) and (12) is isomorphic to a DFN  $\mathcal{F}$ . An implication of that is that for every partition of the graph based on the DFN  $P(F)$ , there is a corresponding unique partition of the DFN  $P(\mathcal{F})$ . This follows directly from the properties of the mapping  $\phi$  being a bijection. Applying  $\phi^{-1}$  to  $P(F)$  defines a unique  $P(\mathcal{F})$ . Therefore, we can partition a DFN using this graph representation. However, we seek to partition the mesh of the DFN, not just the DFN. Let  $G = (V_G, E_G)$  be the graph defined by the conforming Delaunay triangulation of the DFN. Note that with the exception of nodes along the lines of intersection in the DFN, every vertex  $v \in V_G$  corresponds to a node in the mesh that resides on a single fracture  $f_i \in F$ . Let  $f(v) = f_i$  be a function that returns the fracture on which the node corresponding to the vertex  $v$  resides. For nodes on intersections between multiple fractures  $f_i$  and  $f_j$ , let  $f(v) = \min(f_i, f_j)$ .

We define a mapping  $\Pi : G \rightarrow F$  to the graph  $F$

$$\Pi : v_i \in V_F = \{v \in V_G \text{ s.t. } f(v) = f_i\} \quad (14)$$

and

$$\Pi : e_{i,j} \in E_F = \{(f_i, f_j) \text{ if } \exists v \in V_G \text{ s.t. } f(v) = (f_i, f_j)\} \quad (15)$$

Define vertex weights on  $w_v \in V_F$  by (3), the number of nodes in the mesh that reside on each fracture, and the edge weights in  $E_F$  by (4), the number of nodes along the lines of intersections between fractures. Note



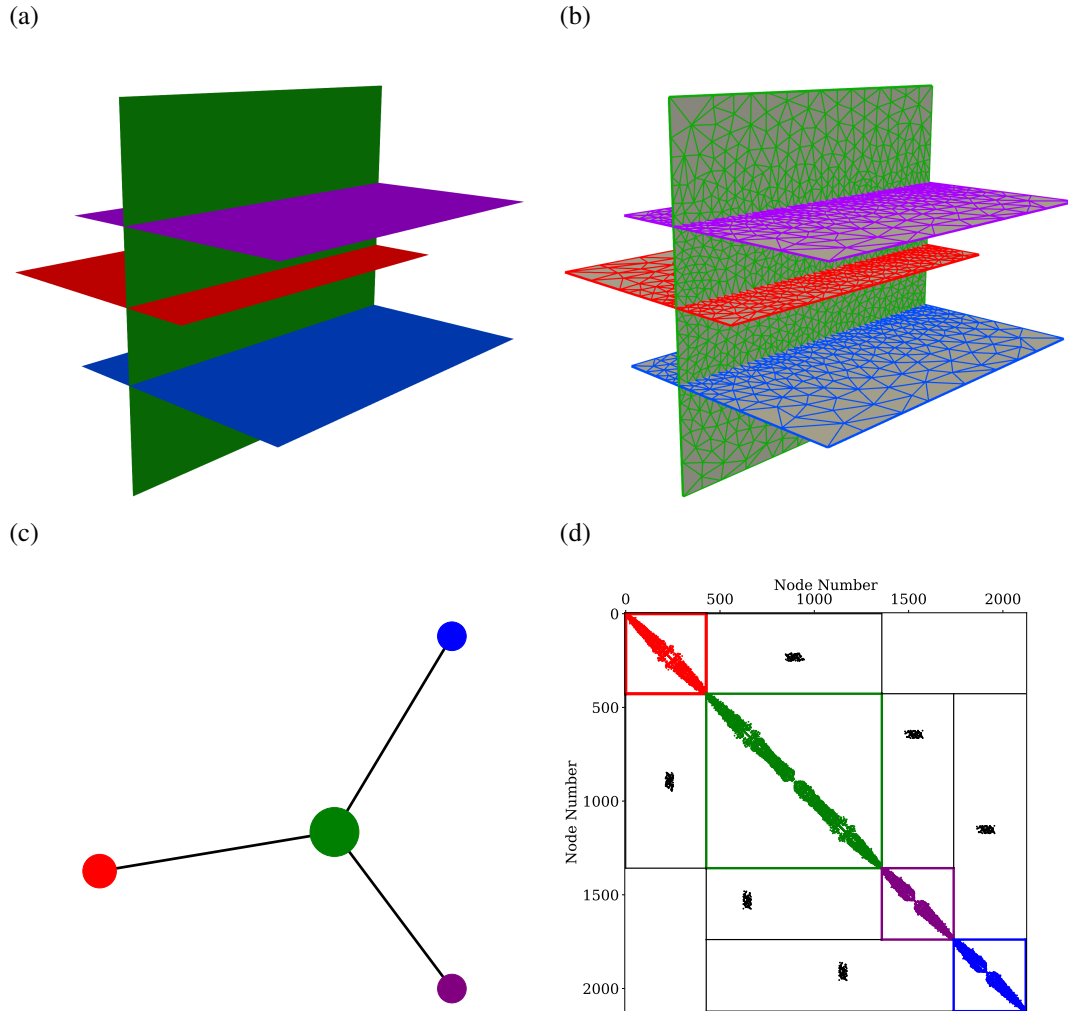


Figure 3: (a) A DFN composed of four fractures. (b) The computational mesh on the DFN. Mesh colors coincide with the fracture on which the mesh node resides. (c) A graph representation of the DFN where vertex colors correspond with the fracture colors in (a). (d) The adjacency matrix for the mesh shown in (c). Colors in the matrix correspond to the fractures on which the nodes reside; black entries correspond to mesh nodes along fracture intersections.

that  $F$  is the graph defined according to equations (10) and (12), the graph based on the topology of the DFN where each vertex corresponds to a fracture and edges indicate that fractures intersect. We retain information about the number of vertices that each coarse node in  $V_F$  represents by using (11) and (13). The graph  $F$  is a coarse version of the mesh-based graph but  $|V_F| \lll |V_G|$  by several orders of magnitude. We can apply the standard multilevel GP method to  $F$  and obtain  $P$  for a  $k$ -way partition. Conceptually, the proposed method defines the first level in the coarsening phase  $\Pi : G_0 \rightarrow G_1 \equiv F$  and then a partition  $P(F)$  is obtained using algorithm 1. Once the partition  $P(F)$  is obtained, we project the the partition onto  $G$  using  $\Pi^{-1}$ . In other words, if a fracture  $f_i \in P_j$ , then all nodes in the mesh on  $f_i$ ,  $f(v) = f_i$ , are placed into  $P_j$  of  $G$ .

**Theorem 4.1.** *The projection of a partition  $P_F$  of the graph  $F = (V_F, E_F)$  defined by equations (10) and (12) onto graph based on the mesh of the DFN  $G = (V_G, E_G)$*

$$\Pi^{-1} : P(F) \rightarrow P(G) \quad (16)$$

*Proof.* By definition every  $v \in V_F$  is in a unique part of the partition  $P$ . Also, note that equation (14) is surjective. Therefore all  $v \in V_G$  in the pre-image of  $v \in V_F$  are in a unique part of the partition  $P$ .  $\square$

Algorithm 2 summarizes the method

**Input:**  $F = (V_F, E_F)$

$\triangleright$  Graph based on DFN

**Output:**  $P(G)$

$\triangleright$  Partition of the mesh of the DFN

$F_0 = F$

$\triangleright$  Initialize Multilevel method with finest level being the DFN based graph

Perform Algorithm 1 to F

1. Coarsening phase : The graph  $F_0$  is transformed into a sequence of smaller graphs  $F_1, F_2, \dots, F_m$  such that  $|V_0| > |V_1| > |V_2| > \dots > |V_m|$
2. Initial partitioning phase: A local refinement algorithm is employed to obtain a  $k$ -way partition  $P_m$  of the graph  $G_m = (V_m, E_m)$
3. Uncoarsening phase: The partition  $P_m$  of  $F_m$  is projected back to  $F_0$  via the intermediate partitions  $P_{m-1}, P_{m-2}, \dots, P_1, P_0$  with subsequent refinements

$\Pi^{-1} : P_0(F_0) \rightarrow P_0(G)$

$\triangleright$  Project the partition of  $F_0$  onto the mesh of the DFN  $G$

**Algorithm 2:** Multilevel Graph Partitioning For DFN

The proposed procedure drastically simplifies the coarsening phase because it reduces the number of steps that need to be taken to reach a graph  $F_m$  where a  $k$ -way partition can be obtained, because the difference in size between  $G$  and  $F$  is large. Moreover, it reduces the the complexity of the uncoarsening phase, because  $P$  only needs to be obtained on  $F$ , not  $G$ . In practice, the mesh  $G$  is never constructed explicitly, only  $F$  needs to be passed to the multilevel GP and the solution passed to the mesh.

As an example, the DFN shown in Fig. 1 is made up of 424 fractures, so the graph-representation has 424 nodes, while the mesh has 870685 nodes for the uniform mesh and 360912 nodes for the variable resolution. Figure 4 (left) shows the graph based on that fracture network  $F$  colored according to a four-way partition. The DFN is shown on the right side of the image, where colors correspond to the partitions in  $F$ , i.e., the mesh is colored by  $P(G)$ . Note that the projection  $\Pi^{-1}$  to obtain the partition  $P(G)$  is agnostic to the meshing strategy and resolution. But, as we shall see in the next section, the meshing strategy does affect the quality of the cut in the projected partition  $P(G)$ .

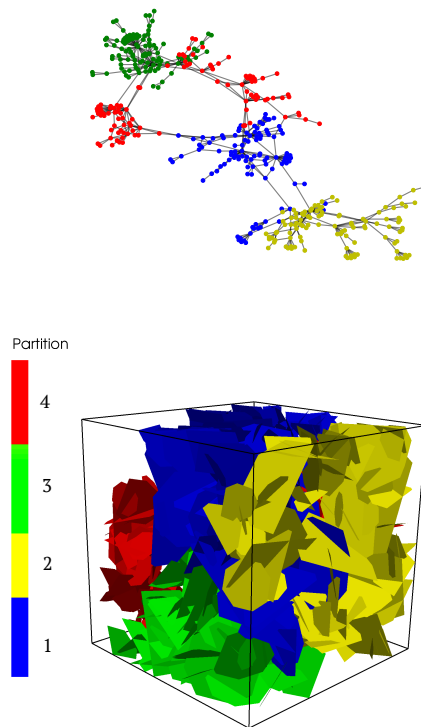


Figure 4: (Top) Graph-representation of the topology of the DFN. (Bottom) DFN colored based on a four-part DFN-based partition. The partition of the mesh (Bottom) is obtained by projecting the partition on the DFN-based graph (Top) onto the mesh.

## 4.2 Numerical Examples

We compare the proposed approach, where the partition of the mesh is based on the partition of the graph representation of the DFN, with the standard approach, where the mesh is partitioned directly. We consider a set of 30 independent identically distributed DFN realizations with both variable and uniform mesh resolution. For each network we consider two partitions: 1) The partition obtained on the mesh itself; we refer to these partitions as  $P'(G)$  and 2) the partition induced from the partition on the graph representation of the DFN  $P'(F)$ . In our experimental results we use the graph partitioning package KaHIP [71] which among other methods implements the Global path algorithm for matching, and flow-based methods for partition refinement. The quality of the partitions are judged by the cut (number of edges that link between partitions) and the imbalance (the difference in sizes of the partitions). We also compare the impact of the partitions on computational performance by solving porous media flow equations, which are Laplace's equation under steady state, and solve for the distribution of pressure within the network. Here, we compare the number of FLOPS, the run time, and number of iterations to obtain the solution using a bi-conjugate gradient scheme with a block Jacobi preconditioner using the PETSC [3] toolkit. The meshes are partitioned into 2, 4, 8, and 16 partitions.

Generation and meshing of the 30 fracture networks is performed using the DFNWORKS computational suite [38]. A conforming Delaunay triangulation on each network is performed using the feature-rejection algorithm for meshing (FRAM) [33]. The parallelized subsurface flow and reactive transport code PFLOTRAN [46] which uses PETSC is applied to obtain the solution to Laplace's equation. The 30 test DFN have fracture lengths that are drawn from a power-law distribution (a commonly observed property in the natural world [6]). Each DFN is constructed in a cubic domain with sides of length 15 m and are composed of circular fractures with uniformly random orientations and uniformly random centers. Fracture radii  $r$  [m] are sampled from a truncated power law distribution with exponent  $\alpha = 2.6$  and upper and lower cutoffs ( $r_u = 5$  m;  $r_0 = 1$  m), with probability density function of

$$p_r(r) = \frac{\alpha}{r_0} \frac{(r/r_0)^{-1-\alpha}}{1 - (r_u/r_0)^{-\alpha}}. \quad (17)$$

The choice of exponent and cut offs are selected such that no single fracture directly connects inflow and outflow boundaries. Variability in hydraulic properties is included into the network by correlating fracture apertures to their radii. We use a positively correlated power-law relationship  $b = \gamma r^\beta$  where  $\gamma = 5.0 \times 10^{-5}$  and  $\beta = 0.5$  are dimensionless parameters.

On average the networks contain around 470 fractures. In the graph representation, there are around 470 nodes and 645 edges. When using a uniform mesh, there are, on average, one million nodes in the mesh (997,221) and nearly two million triangles (1,964,988). The graph based on the uniform mesh is made up of just under one million vertices and close to 3 million edges (2,962,302), on average. Thus, when partitioning the graph based on the uniform mesh there are 2000 times more vertices than when partitioning the graph based solely on the DFN topology. In the case of the variable mesh, there are around half a million nodes (415,206) and three quarter million triangles (836,452), on average. Therefore the graph based on the variable mesh is made up of just under half a million vertices and over one million edges (1,251,751), on average. Thus, when partitioning graph based on the variable mesh there are about 1000 times more vertices than when partitioning the graph based solely on the DFN topology.

### 4.2.1 Partition Quality

We begin by reporting the quality of the partitions and computation time. Table 1 reports the cut, imbalance, and times for the uniform and variable mesh resolution. Reported values are the average of the thirty realizations. Columns correspond to each partition and row are sorted by the number of partitions  $k$ . For the uniform

mesh case, the lowest cuts are all obtained for  $P'(G)$  for all values of  $k$ . The cut values obtained for  $P'(F)$  are about twice as large as those obtained using  $P'(G)$  but partitioning  $P'(G)$  take four orders of magnitude longer than partitioning  $P'(F)$ . The observed difference in cut values for  $P'(F)$  between uniform mesh and variable mesh is due to the different vertex weights in the DFN-based graph, due to different meshes, which results in slightly different partitions. In all cases, the imbalance values are about the same. Similar observations are made in the variable mesh case, but there are a few subtle differences. The difference in the partition quality in terms of the cut between  $P'(G)$  and  $P'(F)$  is substantially larger than in the uniform mesh resolution set. In the case of  $k = 16$ , the cut for  $P'(F)$  is three times larger than for  $P'(G)$ . This increase in the cut values is a result of the fact that cuts in  $P'(F)$  can only occur along intersections in the fracture network mesh, where the mesh is most refined and the highest number of nodes exists. In contrast,  $P'(G)$  is not constrained in this manner and can therefore partition the mesh in region of the fracture where the mesh is coarse and fewer edges exists.

All imbalance values are approximately the same.

Table 1: Partition Metrics

|            |     | Uniform Mesh |         | Variable Mesh |         |
|------------|-----|--------------|---------|---------------|---------|
| Metric     | $k$ | $P'(G)$      | $P'(F)$ | $P'(G)$       | $P'(F)$ |
| Cut        | 2   | 404.73       | 671.67  | 237.20        | 676.37  |
|            | 4   | 941.87       | 1657.30 | 569.03        | 1632.00 |
|            | 8   | 1871.33      | 3412.50 | 1118.30       | 3403.23 |
|            | 16  | 3587.00      | 7503.43 | 2119.90       | 7637.17 |
| Imbalance  | 2   | 0.03         | 0.02    | 0.02          | 0.02    |
|            | 4   | 0.04         | 0.04    | 0.04          | 0.04    |
|            | 8   | 0.05         | 0.04    | 0.05          | 0.04    |
|            | 16  | 0.05         | 0.05    | 0.05          | 0.05    |
| Time [sec] | 2   | 313.84       | 0.13    | 86.68         | 0.13    |
|            | 4   | 375.59       | 0.18    | 93.41         | 0.18    |
|            | 8   | 515.05       | 0.25    | 114.40        | 0.25    |
|            | 16  | 415.08       | 0.35    | 109.10        | 0.35    |

#### 4.2.2 Computational Performance

Table 2 reports the number of GFlops, iterations required for the Krylov solver to converge, and run time using the partitions on the 30 networks. For all values of  $k$ , the selected metrics for the partitions  $P'(G)$  and  $P'(F)$  are roughly the same. An interesting observation is that even though the cuts of  $P'(F)$  are three times larger than those of  $P'(G)$  in the case of the uniform mesh, the run times are only slightly larger. Due to the fewer degrees of freedom in the variable mesh than the uniform mesh, the number of FLOPS, iterations, and solve time are lower than those reported for the uniform mesh. In general, the FLOPS and number of iterations are comparable between  $P'(G)$  and  $P'(F)$ . However, the run times for  $P'(F)$  are slower than for  $P'(G)$ . This slight slow down is likely related to aforementioned issues with the constrained cut location of  $P'(F)$ .

Table 2: Computation Metrics

| Metric     | $k$ | Uniform Mesh |         | Variable Mesh |         |
|------------|-----|--------------|---------|---------------|---------|
|            |     | $P'(G)$      | $P'(F)$ | $P'(G)$       | $P'(F)$ |
| GFlops     | 2   | 45.8         | 44.5    | 12.7          | 12.5    |
|            | 4   | 22.6         | 22.4    | 6.29          | 6.37    |
|            | 8   | 11.3         | 11.6    | 3.24          | 3.21    |
|            | 16  | 5.94         | 5.75    | 1.62          | 1.64    |
| Iterations | 2   | 1223.10      | 1180.20 | 804.03        | 788.13  |
|            | 4   | 1188.97      | 1175.33 | 784.97        | 796.27  |
|            | 8   | 1180.53      | 1211.60 | 806.60        | 799.90  |
|            | 16  | 1236.47      | 1195.17 | 800.87        | 812.83  |
| Time [sec] | 2   | 62.35        | 55.31   | 14.38         | 16.29   |
|            | 4   | 34.94        | 34.98   | 8.45          | 10.10   |
|            | 8   | 21.48        | 22.34   | 5.77          | 6.43    |
|            | 16  | 15.64        | 14.73   | 4.08          | 4.45    |

#### 4.2.3 Total Computational Time

Table 3 reports the total time taken for both the uniform and variable mesh partitions. In all cases, the slowest run times are reported for the  $P'(G)$ , primarily due to the time required for the partition. Note this also drastically affects the scaling of the total run time with number of processors. The fastest times are reported for  $P'(F)$ . Figure 5 also reports these values. The left subplot reports the times required using the mesh for partitioning as shown in blue and DFN-based graph are shown in green; hatched bars are for the uniform mesh and solid bars are the variable mesh. The right subplot is Log-Log plot of the total times corresponding to the one on left. Notice that using the DFN-based partitioning demonstrates good strong scaling, the red dotted line is ideal scaling, with increasing number of CPUs while the mesh based partitioning shows poor scaling with total run time increasing with the number of CPUs.

Table 3: Total Time [sec]

| $k$ | Uniform Mesh |         |               | Variable Mesh |         |               |
|-----|--------------|---------|---------------|---------------|---------|---------------|
|     | $P'(G)$      | $P'(F)$ | $P'(G)/P'(F)$ | $P'(G)$       | $P'(F)$ | $P'(G)/P'(F)$ |
| 2   | 376.19       | 55.44   | 3.74          | 101.06        | 16.42   | 6.15          |
| 4   | 410.53       | 35.16   | 6.64          | 101.86        | 10.28   | 9.90          |
| 8   | 536.53       | 22.59   | 11.48         | 120.17        | 6.68    | 17.98         |
| 16  | 430.72       | 15.07   | 19.97         | 113.11        | 4.80    | 23.56         |

#### 4.2.4 Numerical Examples: Remarks

The examples lead to a few points that are worth discussing.

1. The time required to obtain the partitions using the graph based on the DFN topology is negligible compared to the time required to obtain the partition of the mesh (DFN Delaunay triangulation) due to

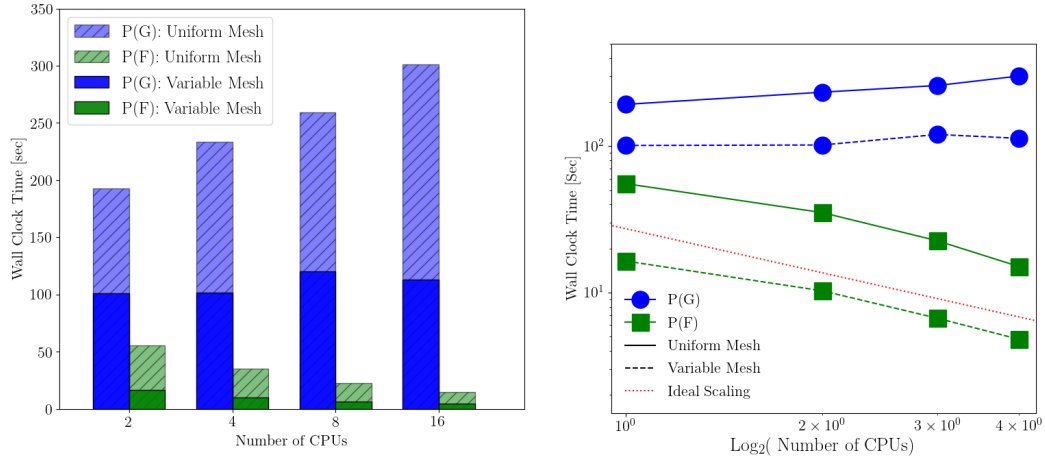


Figure 5: Total time required for partitioning and flow solution. (Left) The times required using the mesh for partitioning are shown in blue and DFN-based graph are in green, hatched bars are for the uniform mesh and solid bars are the variable mesh. (Right) Log-Log plot of the total times corresponding to the one shown on left.

the drastic difference in the size of the corresponding graphs.

2. In terms of cut, the quality of the partition projected down from the DFN onto the mesh depends upon the adopted meshing strategy – uniform resolution or variable resolution. In the case of uniform mesh resolution, the projected cuts are along the intersection lines that are the same resolution as the mesh within the fractures. However, in the case of a variable resolution mesh the projection of the DFN partition onto the mesh requires that the cuts be made along the intersections where mesh resolution is finest. Due to this, the difference between the cut on  $P'(G)$  and  $P'(F)$  is larger than the uniform mesh cases.
3. The quality of the partition influences the requires number of FLOPS, iterations of the Krylov solver, and simulation time. There is little difference in the computational performance between the partitions obtained on the mesh and DFN.
4. The total computational time was either dominated by the partitioning, in the case of mesh based partitioning, or the solver, in the case of the DFN based partitioning. The difference between the relative contribution of partitioning in the two methods are in stark contrast. In the case of the partition based on the mesh, the partitioning was ten to one hundred times slower than the linear solve. In the case of the partition based on the DFN, the partitioning phase was between ten to one hundred times faster. Note that the solver times were generally similar to mesh based partitioning, with the DFN based partition cases being slightly slower than the mesh based partition cases for the variable resolution scenario. These observations result in nearly two orders of magnitude speed up for overall computation when using the DFN based partition.
5. In standard multilevel graph partitioning, there is commonly a step in the uncoarsening phase where local refinements are made to the projected solution from one level higher in the hierarchy. We also applied this concept on the partition of the mesh obtained using the partition of the DFN as an initial

condition. While this slightly improved the cut of the final partition, more so in the variable mesh resolution than for the uniform mesh resolution, it did not significantly affect the total run time (details not included). These insignificant changes indicate that the partition obtained by using projection of the DFN is of sufficient quality to not influence the solver run times.

## 5 Summary and Conclusions

DFN modeling is a powerful tool to improve our understanding of how the multi-scale structure of fractured media influences flow and transport therein. However, the explicit representation of these fracture networks, which contain length scales that range several orders of magnitude, is computationally demanding. As the number of fractures in a DFN increases, so does the size of the mesh and the associated physical systems to model physical phenomena within the DFN. This increase in computational requirements is compounded by the inherent uncertainty in the subsurface that requires numerous realizations of a DFN to bound system behavior. The combination of these facets requires that DFN models utilize efficient HPC methodologies to accelerate system solving time. Load balancing and minimizing communication between processors are key factors in such methodologies. Thus a cornerstone in the use of HPC for DFN simulations is a high-quality partition of the mesh.

We presented a topologically-based method for mesh partitioning in DFN simulations that utilizes the intrinsic multilevel nature of the DFN. The method combines multilevel graph partitioning with a coarse-scale graph representation of the DFN to drastically improve the speed of obtaining a high-quality partition of the DFN mesh. We partitioned the graph based on the DFN, rather than the mesh itself, and partition of the mesh is obtained by projecting the DFN partition onto the mesh. The large difference in size between the graph-based on the mesh and the graph-based on the DFN topology with the DFN based partition lead to a mesh based partition that required a fraction of the time.

We demonstrated the utility of the method by applying it to 30 three-dimensional discrete fracture networks composed of approximately five hundred fractures apiece. We also consider two different DFN meshing strategies. In the first, the mesh has uniform resolution and in the second the resolution of the mesh depends on the distance of the vertex on the fracture from the nearest intersection, with the mesh being finer close to the intersection. We compare the proposed method to standard mesh-based partitioning in terms of graph-based metrics (cut, imbalance, time to obtain the partition), computational-based metrics (FLOPS, iterations, solver time), and total run time. In terms of the graph-based metrics, the results obtained using the DFN-based partition are comparable to those obtained using the mesh-based partition, with the exception of the time required for the partition, which is several orders of magnitude faster in the case of the DFN-based partition. In terms of the computation-based metrics, e.g., solver time and FLOPS, the results are similar as well, depending slightly on the adopted meshing scheme. When combined, the DFN-based partition is therefore several orders of magnitude faster than the mesh-based partition. The results presented here indicate that using the proposed method would reduce the overall time for a single DFN realization simulation and thus allowing for an increase in the number of realizations that can be performed at a fixed computational cost.

The intrinsic multilevel structure of a DFN provides an elegant methodology for efficient and high-quality partitioning of the mesh for computational physics solutions. Multilevel graph partitioning coarsens the mesh until a graph that can be readily partitioned is found. Due to the strong block structure of the mesh and few off diagonal terms, the adopted graph representation is a good proxy for the coarsened version of the computational mesh. Moreover, the proposed methodology for hijacking multilevel graph partitioning could be applied to any system that exhibits such a structure and is thus amenable to a coarse-scale graph representation.



## Acknowledgments

This work was funded by the Department of Energy at Los Alamos National Laboratory through the Laboratory-Directed Research and Development Program LANL-LDRD grant #20170103DR. J.D.H. acknowledges support from the LANL LDRD program office Grant Number # 20180621ECR. This work was supported in part by the National Science Foundation under the Grant No. 1522751.

## References

- [1] Garrett Aldrich, Jeffrey D Hyman, Satish Karra, Carl W Gable, Nataliia Makedonska, Hari Viswanathan, Jonathan Woodring, and Bernd Hamann. Analysis and visualization of discrete fracture networks using a flow topology graph. *IEEE transactions on visualization and computer graphics*, 23(8):1896–1909, 2017.
- [2] Christian André Andresen, Alex Hansen, Romain Le Goc, Philippe Davy, and Sigmund Mongstad Hope. Topology of fracture networks. *Frontiers in Physics*, 1:Art–7, 2013.
- [3] Satish Balay, Shrirang Abhyankar, Mark Adams, Jed Brown, Peter Brune, Kris Buschelman, LD Dalcin, Victor Eijkhout, W Gropp, Dinesh Kaushik, et al. PETSC users manual revision 3.8. Technical report, Argonne National Lab.(ANL), Argonne, IL (United States), 2017.
- [4] Stefano Berrone, Sandra Pieraccini, and Stefano Scialo. A pde-constrained optimization formulation for discrete fracture network flows. *SIAM J. Sci. Comput.*, 35(2):B487–B510, 2013.
- [5] Stefano Berrone, Sandra Pieraccini, Stefano Scialò, and Fabio Vicini. A parallel solver for large scale dfn flow simulations. *SIAM J. Sci. Comput.*, 37(3):C285–C306, 2015.
- [6] Eric Bonnet, Olivier Bour, Noelle E Odling, Philippe Davy, Ian Main, Patience Cowie, and Brian Berkowitz. Scaling of fracture systems in geological media. *Reviews of Geophysics*, 39(3):347–383, 2001.
- [7] Achi Brandt and Dorit Ron. Multigrid solvers and multilevel optimization strategies. In *Multilevel optimization in VLSICAD*, pages 1–69. Springer, 2003.
- [8] Thang Nguyen Bui and Curt Jones. A heuristic for reducing fill-in in sparse matrix factorization. Technical report, Society for Industrial and Applied Mathematics (SIAM), Philadelphia, PA (United States), 1993.
- [9] Aydın Buluç, Henning Meyerhenke, Ilya Safro, Peter Sanders, and Christian Schulz. Recent advances in graph partitioning. In *Algorithm Engineering*, pages 117–158. Springer, 2016.
- [10] M. C. Cacas, E. Ledoux, G. De Marsily, A. Barbreau, P. Calmels, B. Gaillard, and R. Margritta. Modeling fracture flow with a stochastic discrete fracture network: Calibration and validation: 2. The transport model. *Water Resour. Res.*, 26(3):491–500, 1990.
- [11] C-K Cheng and Y-CA Wei. An improved two-way partitioning algorithm with stable performance (vlsi). *IEEE Transactions on Computer-Aided Design of Integrated Circuits and Systems*, 10(12):1502–1511, 1991.
- [12] Cédric Chevalier and Ilya Safro. Comparison of coarsening schemes for multilevel graph partitioning. In *International Conference on Learning and Intelligent Optimization*, pages 191–205. Springer, 2009.

- [13] Philippe Davy, Romain Le Goc, and Caroline Darcel. A model of fracture nucleation, growth and arrest, and consequences for fracture density and scaling. *J. Geophys. Res.-Sol. Ea.*, 118(4):1393–1407, 2013.
- [14] J-R de Dreuzy, C Darcel, P Davy, and O Bour. Influence of spatial correlation of fracture centers on the permeability of two-dimensional fracture networks following a power law length distribution. *Water Resour. Res.*, 40(1), 2004.
- [15] J.-R. de Dreuzy, Y. Méheust, and G. Pichot. Influence of fracture scale heterogeneity on the flow properties of three-dimensional discrete fracture networks. *J. Geophys. Res.-Sol. Ea.*, 117(B11), 2012.
- [16] WS Dershowitz and C Fidelibus. Derivation of equivalent pipe network analogues for three-dimensional discrete fracture networks by the boundary element method. *Water Resour. Res.*, 35(9):2685–2691, 1999.
- [17] J Erhel, J-R de Dreuzy, and B Poirriez. Flow simulation in three-dimensional discrete fracture networks. *SIAM J. Sci. Comput.*, 31(4):2688–2705, 2009.
- [18] Robert Eymard, Thierry Gallouët, and Raphaële Herbin. Finite volume methods. *Handbook of numerical analysis*, 7:713–1018, 2000.
- [19] Charles M Fiduccia and Robert M Mattheyses. A linear-time heuristic for improving network partitions. In *Papers on Twenty-five years of electronic design automation*, pages 241–247. ACM, 1988.
- [20] Andrew Frampton and V Cvetkovic. Inference of field-scale fracture transmissivities in crystalline rock using flow log measurements. *Water Resour. Res.*, 46(11), 2010.
- [21] Jörn Garbers, Hans Jurgen Promel, and Angelika Steger. Finding clusters in vlsi circuits. In *1990 IEEE International Conference on Computer-Aided Design*, pages 520–523. IEEE, 1990.
- [22] Michael R Garey, David S Johnson, and Larry Stockmeyer. Some simplified np-complete problems. In *Proceedings of the sixth annual ACM symposium on Theory of computing*, pages 47–63. ACM, 1974.
- [23] HH Gerke and M Th Van Genuchten. A dual-porosity model for simulating the preferential movement of water and solutes in structured porous media. *Water Resour. Res.*, 29(2):305–319, 1993.
- [24] Teklu Hadgu, Satish Karra, Elena Kalinina, Nataliia Makedonska, Jeffrey D. Hyman, Katherine Klise, Hari S. Viswanathan, and Yifeng Wang. A comparative study of discrete fracture network and equivalent continuum models for simulating flow and transport in the far field of a hypothetical nuclear waste repository in crystalline host rock. *Journal of Hydrology*, 553:59 – 70, 2017.
- [25] Lars Hagen and Andrew B Kahng. A new approach to effective circuit clustering. In *Proceedings of the 1992 IEEE/ACM international conference on Computer-aided design*, pages 422–427. IEEE Computer Society Press, 1992.
- [26] William W Hager, James T Hungerford, and Ilya Safro. A multilevel bilinear programming algorithm for the vertex separator problem. *Computational Optimization and Applications*, 69(1):189–223, 2018.
- [27] Bruce Hendrickson and Robert Leland. A multi-level algorithm for partitioning graphs. 1995.
- [28] Sigmund Mongstad Hope, Philippe Davy, Julien Maillot, Romain Le Goc, and Alex Hansen. Topological impact of constrained fracture growth. *Frontiers in Physics*, 3:75, 2015.
- [29] YF Hu and Jennifer A Scott. A multilevel algorithm for wavefront reduction. *SIAM Journal on Scientific Computing*, 23(4):1352–1375, 2001.

- [30] O Huseby, JF Thovert, and PM Adler. Geometry and topology of fracture systems. *J. Phys A-Math Gen*, 30(5):1415, 1997.
- [31] Laurent Hyafil and Ronald L Rivest. *Graph partitioning and constructing optimal decision trees are polynomial complete problems*. IRIA. Laboratoire de Recherche en Informatique et Automatique, 1973.
- [32] J. D. Hyman, M. Dentz, A. Hagberg, and P. Kang. Linking structural and transport properties in three-dimensional fracture networks. *J. Geophys. Res. Sol. Ea.*, 2019.
- [33] J. D. Hyman, C. W. Gable, S. L. Painter, and N. Makedonska. Conforming Delaunay triangulation of stochastically generated three dimensional discrete fracture networks: A feature rejection algorithm for meshing strategy. *SIAM J. Sci. Comput.*, 36(4):A1871–A1894, 2014.
- [34] J. D. Hyman, A. Hagberg, G. Srinivasan, J. Mohd-Yusof, and H. Viswanathan. Predictions of first passage times in sparse discrete fracture networks using graph-based reductions. *Phys. Rev. E*, 96:013304, Jul 2017.
- [35] J. D. Hyman and J. Jiménez-Martínez. Dispersion and mixing in three-dimensional discrete fracture networks: Nonlinear interplay between structural and hydraulic heterogeneity. *Water Resources Research*, 54(5):3243–3258, 2018.
- [36] JD Hyman, J Jiménez-Martínez, HS Viswanathan, JW Carey, ML Porter, E Rougier, S Karra, Q Kang, L Frash, L Chen, et al. Understanding hydraulic fracturing: a multi-scale problem. *Phil. Trans. R. Soc. A*, 374(2078):20150426, 2016.
- [37] Jeffrey D Hyman, Aric Hagberg, Dave Osthus, Shriram Srinivasan, Hari Viswanathan, and Gowri Srinivasan. Identifying backbones in three-dimensional discrete fracture networks: A bipartite graph-based approach. *Multiscale Modeling & Simulation*, 16(4):1948–1968, 2018.
- [38] Jeffrey D Hyman, Satish Karra, Nataliia Makedonska, Carl W Gable, Scott L Painter, and Hari S Viswanathan. dfnWorks: A discrete fracture network framework for modeling subsurface flow and transport. *Comput. Geosci.*, 84:10–19, 2015.
- [39] C. Jenkins, A. Chadwick, and S. D Hovorka. The state of the art in monitoring and verification—ten years on. *Int. J. Greenh. Gas. Con.*, 40:312–349, 2015.
- [40] Steven Joyce, Lee Hartley, David Applegate, Jaap Hoek, and Peter Jackson. Multi-scale groundwater flow modeling during temperate climate conditions for the safety assessment of the proposed high-level nuclear waste repository site at Forsmark, Sweden. *Hydrogeol. J.*, 22(6):1233–1249, 2014.
- [41] S Karra, N Makedonska, HS Viswanathan, SL Painter, and JD Hyman. Effect of advective flow in fractures and matrix diffusion on natural gas production. *Water Resour. Res.*, 51(10):8646–8657, 2015.
- [42] George Karypis and Vipin Kumar. A fast and high quality multilevel scheme for partitioning irregular graphs. *SIAM Journal on scientific Computing*, 20(1):359–392, 1998.
- [43] B. W. Kernighan and S. Lin. An efficient heuristic procedure for partitioning graphs. *The Bell System Technical Journal*, 49(2):291–307, Feb 1970.
- [44] Bernard H Kueper and David B McWhorter. The behavior of dense, nonaqueous phase liquids in fractured clay and rock. *Ground Water*, 29(5):716–728, 1991.
- [45] Vipin Kumar, Ananth Grama, Anshul Gupta, and George Karypis. *Introduction to parallel computing: design and analysis of algorithms*, volume 400. Benjamin/Cummings Redwood City, 1994.

- [46] P.C. Lichtner, G.E. Hammond, C. Lu, S. Karra, G. Bisht, B. Andre, R.T. Mills, and J. Kumar. PFLOTRAN user manual: A massively parallel reactive flow and transport model for describing surface and subsurface processes. Technical report, (Report No.: LA-UR-15-20403) Los Alamos National Laboratory, 2015.
- [47] Peter Lichtner and Satish Karra. Modeling multiscale-multiphase-multicomponent reactive flows in porous media: Application to co2 sequestration and enhanced geothermal energy using PFLOTRAN. In *Al-Khoury, R., Bundschuh, J. (eds.) Computational Models for CO2 Geo-sequestration & Compressed Air Energy Storage (<http://www.crcnetbase.com/doi/pdfplus/10>)*, pages 81–136. CRC Press, 2014.
- [48] JCS Long, JS Remer, CR Wilson, and PA Witherspoon. Porous media equivalents for networks of discontinuous fractures. *Water Resour. Res.*, 18(3):645–658, 1982.
- [49] Julien Maillot, Philippe Davy, Romain Le Goc, Caroline Darcel, and Jean-Raynald De Dreuzy. Connectivity, permeability, and channeling in randomly distributed and kinematically defined discrete fracture network models. *Water Resour. Res.*, 52(11):8526–8545, 2016.
- [50] N. Makedonska, J. D. D Hyman, S. Karra, S. L Painter, C. W. W Gable, and H. S Viswanathan. Evaluating the effect of internal aperture variability on transport in kilometer scale discrete fracture networks. *Adv. Water Resour.*, 94:486–497, 2016.
- [51] Nashat Mansour, Ravi Ponnusamy, A Choudhary, and Geoffrey C Fox. Graph contraction for physical optimization methods: a quality-cost tradeoff for mapping data on parallel computers. In *Proceedings of the 7th international conference on Supercomputing*, pages 1–10. ACM, 1993.
- [52] Henning Meyerhenke, Burkhard Monien, and Thomas Sauerwald. A new diffusion-based multilevel algorithm for computing graph partitions. *Journal of Parallel and Distributed Computing*, 69(9):750–761, 2009.
- [53] RS Middleton, JW Carey, RP Currier, JD Hyman, Q Kang, S Karra, J Jiménez-Martínez, ML Porter, and HS Viswanathan. Shale gas and non-aqueous fracturing fluids: Opportunities and challenges for supercritical CO<sub>2</sub>. *Appl. Energ.*, 147:500–509, 2015.
- [54] Michael Murphy, David M Mount, and Carl W Gable. A point-placement strategy for conforming Delaunay tetrahedralization. *International Journal of Computational Geometry & Applications*, 11(06):669–682, 2001.
- [55] H. Mustapha and K. Mustapha. A new approach to simulating flow in discrete fracture networks with an optimized mesh. *SIAM J. Sci. Comput.*, 29:1439, 2007.
- [56] Hussein Mustapha, Roussos Dimitrakopoulos, Thomas Graf, and Abbas Firoozabadi. An efficient method for discretizing 3d fractured media for subsurface flow and transport simulations. *International Journal for Numerical Methods in Fluids*, 67(5):651–670, 2011.
- [57] National Research Council. *Rock fractures and fluid flow: contemporary understanding and applications*. National Academy Press, 1996.
- [58] Shlomo P Neuman and Joseph S Depner. Use of variable-scale pressure test data to estimate the log hydraulic conductivity covariance and dispersivity of fractured granites near oracle, arizona. *J. Hydrol.*, 102(1-4):475–501, 1988.
- [59] S.P. Neuman. Trends, prospects and challenges in quantifying flow and transport through fractured rocks. *Hydrogeol. J.*, 13(1):124–147, 2005.

- [60] A. Wille Nordqvist, Y. W. Tsang, C. F. Tsang, Björn Dverstorp, and Johan Andersson. A variable aperture fracture network model for flow and transport in fractured rocks. *Water Resources Research*, 28(6):1703–1713, 1992.
- [61] G Pichot, J Erhel, and J-R de Dreuzy. A mixed hybrid mortar method for solving flow in discrete fracture networks. *Appl. Anal.*, 89(10):1629–1643, 2010.
- [62] G Pichot, J Erhel, and J-R de Dreuzy. A generalized mixed hybrid mortar method for solving flow in stochastic discrete fracture networks. *SIAM J. Sci. Comput.*, 34(1):B86–B105, 2012.
- [63] Karsten Pruess, Curtis M Oldenburg, and GJ Moridis. Tough2 user’s guide version 2. 1999.
- [64] M Cecilia Rivara. Algorithms for refining triangular grids suitable for adaptive and multigrid techniques. *International journal for numerical methods in Engineering*, 20(4):745–756, 1984.
- [65] Maria-Cecilia Rivara. Mesh refinement processes based on the generalized bisection of simplices. *SIAM Journal on Numerical Analysis*, 21(3):604–613, 1984.
- [66] Dorit Ron, Ilya Safro, and Achi Brandt. Relaxation-based coarsening and multiscale graph organization. *Multiscale Modeling & Simulation*, 9(1):407–423, 2011.
- [67] Ilya Safro, Dorit Ron, and Achi Brandt. Graph minimum linear arrangement by multilevel weighted edge contractions. *Journal of Algorithms*, 60(1):24–41, 2006.
- [68] Ilya Safro, Dorit Ron, and Achi Brandt. Multilevel algorithms for linear ordering problems. *Journal of Experimental Algorithmics (JEA)*, 13:4, 2009.
- [69] Ilya Safro, Peter Sanders, and Christian Schulz. Advanced coarsening schemes for graph partitioning. *Journal of Experimental Algorithmics (JEA)*, 19:2–2, 2015.
- [70] Peter Sanders and Christian Schulz. Engineering multilevel graph partitioning algorithms. In *European Symposium on Algorithms*, pages 469–480. Springer, 2011.
- [71] Peter Sanders and Christian Schulz. Think locally, act globally: Highly balanced graph partitioning. In *International Symposium on Experimental Algorithms*, pages 164–175. Springer, 2013.
- [72] Gowri Srinivasan, Jeffrey D Hyman, David A Osthus, Bryan A Moore, Daniel O’Malley, Satish Karra, Esteban Rougier, Aric A Hagberg, Abigail Hunter, and Hari S Viswanathan. Quantifying topological uncertainty in fractured systems using graph theory and machine learning. *Scientific reports*, 8(1):11665, 2018.
- [73] YW Tsang, CF Tsang, FV Hale, and B Dverstorp. Tracer transport in a stochastic continuum model of fractured media. *Water Resour. Res*, 32(10):3077–3092, 1996.
- [74] Manuel Valera, Zhengyang Guo, Priscilla Kelly, Sean Matz, Vito Adrian Cantu, Allon G. Percus, Jeffrey D. Hyman, Gowri Srinivasan, and Hari S. Viswanathan. Machine learning for graph-based representations of three-dimensional discrete fracture networks. *Computational Geosciences*, Jan 2018.
- [75] JE VanderKwaak and EA Sudicky. Dissolution of non-aqueous-phase liquids and aqueous-phase contaminant transport in discretely-fractured porous media. *J. Contam. Hydrol.*, 23(1-2):45–68, 1996.
- [76] H. S. Viswanathan, Hyman J.D., S. Karra, D. O’Malley, S. Srinivasan, A. Hagberg, and G. Srinivasan. Advancing graph-based algorithms for predicting flow and transport in fractured rock. *Water Resour. Res.*, 2018.

- [77] Chris Walshaw and Mark Cross. Mesh partitioning: a multilevel balancing and refinement algorithm. *SIAM Journal on Scientific Computing*, 22(1):63–80, 2000.
- [78] Robert W Zimmerman, Gang Chen, Teklu Hadgu, and Gudmundur S Bodvarsson. A numerical dual-porosity model with semianalytical treatment of fracture/matrix flow. *Water Resour. Res.*, 29(7):2127–2137, 1993.
- [79] G Zyvoloski. FEHM: A control volume finite element code for simulating subsurface multi-phase multi-fluid heat and mass transfer. *Los Alamos Unclassified Report LA-UR-07-3359*, 2007.